XX IMEKO World Congress
Metrology for Green Growth
September 9–14, 2012, Busan, Republic of Korea

THERMOPOWER MEASUREMENT OF SINGLE NANOWIRE USING A MEMS DEVICE

[1]Ho Sun Shin, [1]Joon Sung Lee, [2]Seong Gi Jeon, [2]Jin Yu, and [1]Jae Yong Song

[1]Korea Research Institute of Standards and Science, Daejon, Republic of Korea, 305-340
[2]Korea Advanced Institute of Science and Technology, Daejon, Republic of Korea, 305-701

Abstract: We have fabricated a MEMS device on suspended silicon nitride in order to measure the thermoelectric properties of single nanowire. The temperature gradient was generated by a nanoheater and the temperatures of thermometers were calibrated and measured. Seebeck coefficient and electrical conductivity of single Bi_2Te_3 nanowire with a 70 nm-diameter were measured in the temperature range of 50 K to 400 K. Based on the simulation results of the temperature distribution over the MEMS structure, the method of calibrating the temperature and measurement uncertainty are discussed.

Keywords: nanowire, MEMS, thermal simulation, thermopower

1. INTRODUCTION

One-dimensional nanostructures have extensively attracted much attention because they have unique physical properties different from their bulk properties. Regarding thermoelectrics, size-effect and quantum confinement effect are expected to increase the figures of merit for nanostructured thermoelectric (TE) materials such as quantum dots, superlattices, and nanowires (NWs) [1]. Among TE materials, Bi_2Te_3 (BT) is one of the most promising candidates for TE devices due to its high figure of merit near room temperature.

The efficiency of a thermoelectric material is determined by a dimensionless thermoelectric figure of merit, ZT. The figure of merit is defined by

$$ZT = S^2\sigma/k$$

where S is thermoelectric power (Seebeck coefficient), σ electrical conductivity, and k thermal conductivity. To determine the Seebeck coefficient, $S=\Delta V/\Delta T$, it is required to measure the thermoelectric voltage ΔV and the temperature gradient, ΔT, simultaneously. To realize this measurement for one-dimensional nanostructures, we developed a MEMS-based platform, on which the thermopower and the electrical conductivity of one-dimensional structure can be measured at the same time. Temperature gradient, ΔT, was generated by Joule heating of the Pt nanoheaters while the thermoelectric voltage was measured with a nanovoltmeter. The electrical conductivity of a NW was measured using the four-point probe technique.

2. FABRICATION OF THERMOELECTRIC MEMS DEVICE

The substrate was prepared by depositing 50 nm-thick low-stress silicon nitride on top of a 6-inch silicon wafer covered by a 300 nm-thick silicon oxide layer. A micro-sized electrode pattern was defined by a conventional photolithography which was followed by an e-beam evaporation of metals and a lift-off process. This micro-pattern was used as linking electrodes connecting the MEMS to external measurement equipment. The thickness of the micro-pattern electrode was 200 nm, which consists of 155 nm of Au and 45 nm of Ti. E-beam lithography technique was adopted to form a nanopattern, which consisted of symmetric pairs of a Pt nanoheater, a current carrying electrode, and a Pt thermometer placed sequentially towards the center. The Pt thermometers positioned close to the center were also used as the voltage measurement probes for the 4-probe electrical conductivity measurements. The Pt line width was designed to be 1 μm and 0.5 μm for the thermometers and the nanoheaters, respectively. The nanopattern metal consisted of 90 nm-thick Pt on top of 10 nm-thick Ti used as an adhesion layer. The backside silicon beneath the nanopattern was etched away by an anisotropic wet etching process to realize a suspended MEMS structure, leaving only the silicon nitride/oxide layer of 50/300 nm thickness to enhance the measurement sensitivity. Figure 1 is a schematic diagram of the MEMS fabrication process and Figure 2 shows the nanopattern at the center of the MEMS structure.

To make the electric and thermal contacts between a single BT NW and the Pt electrodes, we used Ni/Al layer as the contact material. After spin-coating with Polymethylmethacrylate (PMMA, 950 k, 4 %), the substrates were soft-baked at 170℃ for 2 min on a hot plate. E-beam lithography was performed around the NW in selected area, and then the development was carried out in MIBK 1:3 solution. Ni (10 nm) and Al (120 nm) films were deposited by RF-sputtering system. Finally, the Ni/Al film was peeled off from the unwanted area on the Si chip by a lift-off process in boiled acetone.

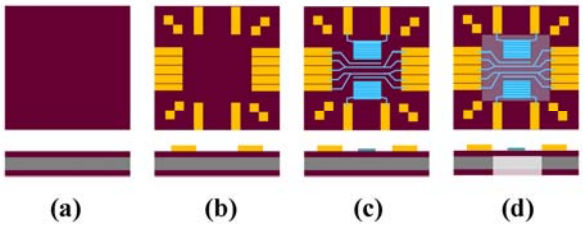

Figure 1. A schematic diagram of MEMS fabrication process. (a) Silicon nitride/oxide layer on both sides of the Si wafer, (b) micropatterning (Au), (c) nanopatterning (Pt), (d) back side dry / wet etching

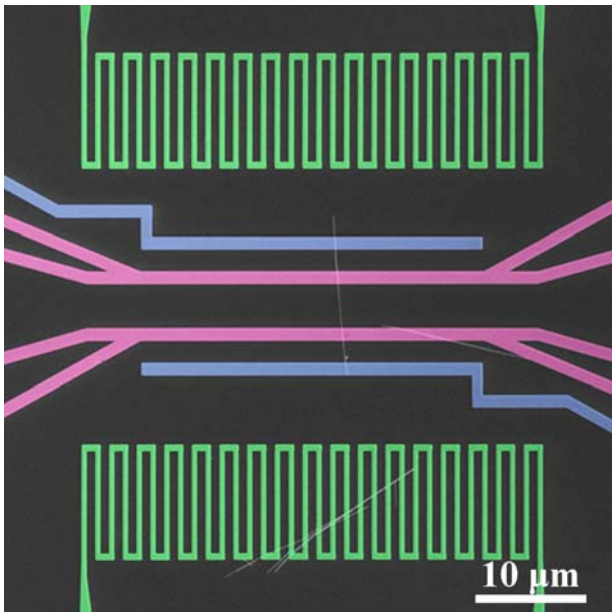

Figure 2. A SEM image (false color) of a thermoelectric MEMS device. A pair of nanoheaters (green color) is shown at the top and the bottom. The inner electrodes (purple) are used as thermometers. Four-point electrical contacts with a NW can be configured with the inner and the outer (blue) electrodes. A single bismuth telluride NW is shown at the center.

3. CALIBRATION OF TEMPERATURE

The temperature difference between the voltage contacts of a NW was obtained from the resultant response of the thermometers in electrical resistance variation. We determined the temperature coefficient of resistance (TCR) from the resistance versus temperature plot in the range of 50 K to 400 K. This process was carried out while decreasing the temperature in order to avoid annealing effect in the Pt thermometers. We measured the TCR for each individual MEMS specimen before thermoelectric measurement for accuracy. Figure 3 is the temperature vs. resistance plot. The linear slope was fitted well with $R^2 \sim 0.999$. The average TCR value of the MEMS was (0.1428±0.0003) Ω/K.

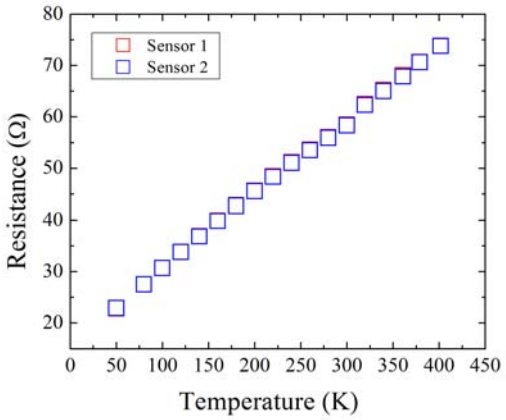

Figure 3. The resistance change with temperature in each individual Pt sensor

4. MEASUREMENT OF THERMOPOWER AND ELECTRIC CONDUCTIVITY

Thermopower measurement of a single NW has been carried out in the range of 50 to 400 K. The temperature gradient generated using a dc current (Keithley, 6220) through one nanoheater and the corresponding thermoelectric voltage was recorded by a nanovoltmeter (Keithley, 2182A). Two lock-in amplifiers (Signal recovery, 5210) simultaneously red the resistance of both thermometers (inner electrodes). A switching module (scanner relay) made it possible that the measurements of the temperatures by the lock-in units (ΔT) and of the thermoelectric potential difference by the nanovoltmeter (ΔV) be carried out on the same inner electrodes. One lock-in unit measured the ac voltage at 31.1 Hz for one thermometer. The other lock-in unit performed the same measurement for the other thermometer at 40.5 Hz.

In order to confirm that the measured thermoelectric voltage under a given temperature gradient resulted from thermoelectric effect only, the same measurement was performed using the other heater. If the measured voltage value is due to thermoelectric effect only, the voltage value measured with the reversed thermal gradient should have the same magnitude with the opposite polarity. In this step, we noted that the position of a NW can be an error source due to non-uniform thermal distribution along the thermometers. This possible error source will be discussed in the following simulation part. Another validity check is to reverse the current direction in the nanoheaters. This should yield the same result as before. Figure 4 shows the thermoelectric voltage variation occurring as the heater power is changed stepwise.

The electrical conductivity of a single NW was measured using four-point probe method. The outer electrodes were used as dc current source and drain. The voltage drop was measured between the inner electrodes. Figure 5 shows ohmic behaviour and the conductance can be obtained from this I-V slope. The electrical conductivity can be calculated

using the dimension of the NW determined by a SEM observation.

The thermopower and the electrical conductivity of a single BT NW are shown in Figures 5 and 6, respectively.

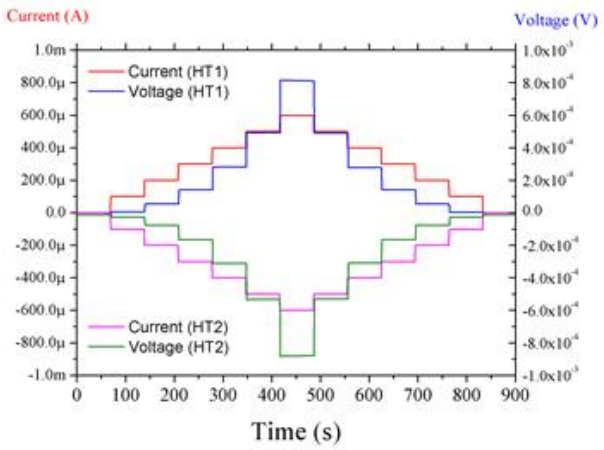

Figure 4. Thermoelecric voltage variation occurring as the heater power is changed stepwise. Similar magnitude but opposite polarity shows that these results are attributed to thermoelectric effect.

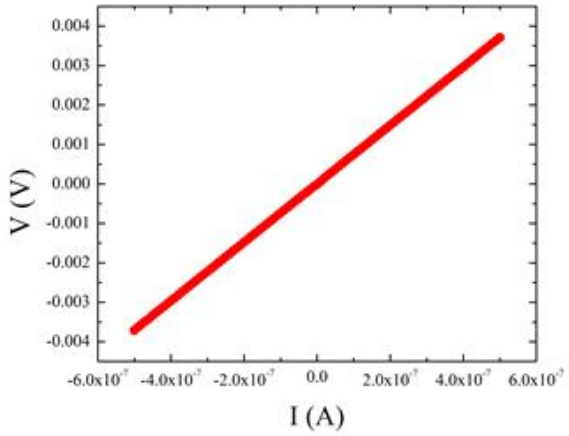

Figure 5. Four-point I-V characteristic from a single NW

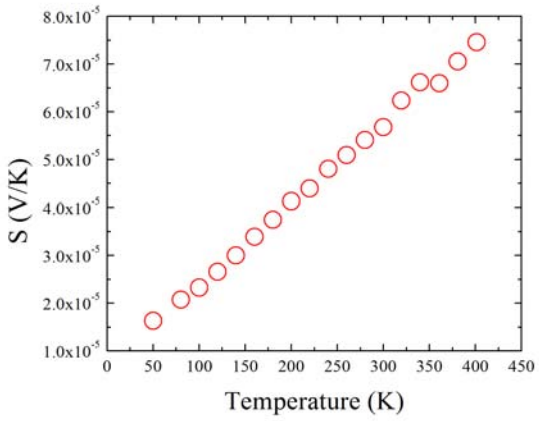

Figure 6. Thermopower measurement result for a single BT NW

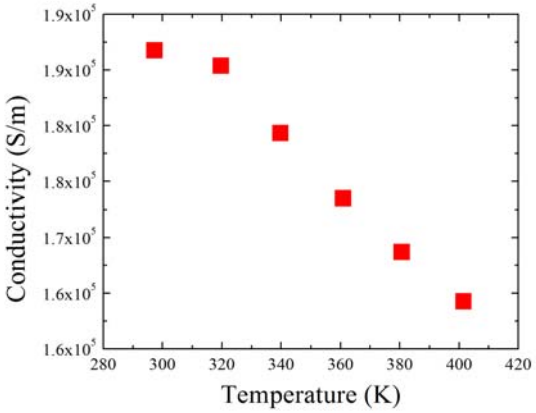

Figure 7. Electrical conductivity plot for a single BT NW

4. SIMULATION OF TEMPERATURE DISTRIBUTION

Since the heaters and temperature sensors are placed on a solid membrane instead of a long bridge structure, the temperature distribution along the sensors cannot be uniform. To analyze this issue, a static thermal simulation on the structure was carried out using a commercial finite element simulation package (Ansoft Maxwell 3D). The simulation model was made to have the same nominal dimensions with the membrane template used in the experiments, except that the silicon substrate facing the heat sink was reduced in the simulation model. This reduction in the substrate thickness does not produce any appreciable error in the simulation results because of the high thermal conductivity and the wide heat path of the etched silicon support. The thermal conductivity values of the materials were simply given as constants without temperature dependence (low-stress silicon nitride: 3 W/m·K [2], silicon oxide: 1.5 W/m·K, thin film Pt: 63 W/m·K [3], silicon substrate: 148 W/m·K), and the heat sink temperature was set to 0°C for convenience. Heat transfer via radiation and convection should be negligible for our measurement conditions (P ~ 10 mTorr, T < 400 K), and thus was not included in the simulation.

In the simulation, a dc current of 200 μA was supplied to heater 1 (R_h ~ 1.5 kΩ), which resulted in a total heat power of ~60 μW. The computed temperature distribution on the membrane is shown in Figure 8. The influence of the Pt electrode pattern can be seen on the image: because of the higher thermal conductivity of Pt, the temperature distribution along the Pt pattern tends to be a little bit equalized. However, the temperature distribution on the sensors does not much deviate from the overall trend.

According to the measurement scheme, the temperature of a sensor is deduced from the measured 4-probe resistance of the Pt line. Assuming a linear dependence of the sheet resistance of the Pt line on the local temperature, the measured resistance can be directly converted to the average temperature of the sensor by the R versus T relationship obtained beforehand. However, since the temperature along the Pt line is not uniform, the exact nodal temperature of the

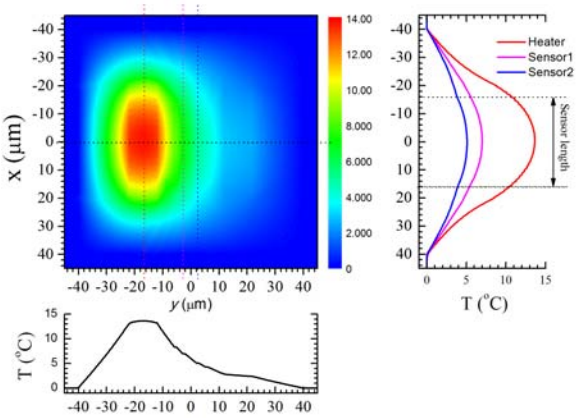

Figure 8. Simulated temperature distribution on the m embrane structure. The Si substrate below the square re gion [–40 : *x* and *y* : +40 μm] was etched away. The temp erature outside of the etch boundary turned out to be al most 0 degree as shown in the color map. The computed temperature distribution along each of the dotted lines (r ed: middle of the heater, purple: hot-side sensor, blue: co ld-side sensor) are shown in the left side and the bottom graphs.

NW of which the thermoelectric voltage is being measured cannot be obtained simply. This problem can be solved referring to Figure 9 where the local temperature distribution along the sensors is given with respect to their average temperatures. According to Figure 9, the local temperatures at the sensor center and ends are roughly 9 % higher and 17 % lower than the average values for each sensor, respectively. The slight asymmetry with respect to the sensor center is due to the asymmetrically designed current leads for NWs. The deviation ratio given in Figure 9 should remain the same regardless of the absolute heating power level. With the help of this data, the local temperatures of the NW contact nodes can be obtained from the measured average temperature values.

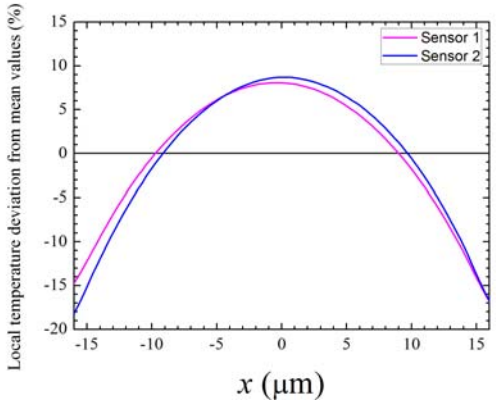

Figure 9. Local temperature deviation from the mean values computed on the sensor strips.

It is important to note that since the deviation values in Figure 9 are from the mean temperatures of the sensors, the actual temperature difference between the hot and cold nodes of the NW may deviate much larger than by the values shown. According to the simulation result, the average temperature of the cold-side sensor subtracted by the ambient temperature is ~72 % of that of the hot-side sensor ($\Delta T_{\text{cold\_avg}} \sim 0.72\Delta T_{\text{hot\_avg}}$). Suppose an extreme case that a NW is placed between one end of the hot-side sensor and the center of the cold-side sensor. $\Delta T_{\text{hot}}(x_{\text{hot}}) \sim 0.83\Delta T_{\text{hot\_avg}}$ and $\Delta T_{\text{cold}}(x_{\text{cold}}) \sim 1.09\Delta T_{\text{cold\_avg}} \sim 0.78\Delta T_{\text{hot\_avg}}$ from the data in Figure 9. Then, the actual temperature difference between the nodes becomes $\Delta T_{\text{hot}}(x_{\text{hot}}) - \Delta T_{\text{cold}}(x_{\text{cold}}) \sim 0.045\Delta T_{\text{hot\_avg}}$, instead of the measured value $\Delta T_{\text{hot\_avg}} - \Delta T_{\text{cold\_avg}} \sim 0.28\Delta T_{\text{hot\_avg}}$. It means that, for this extreme case, the actual temperature difference between the sensor contacts on the NW can be mere ~16 % of the difference between the measured average temperatures of the sensors.

5. SUMMARY

We have fabricated a MEMS device for thermoelectric measurement of a single NW. The MEMS device was validated by calibrating the nanoheaters, thermometers and by formation of ohmic contacts. We measured thermopower and electrical conductivity of a single BT NW with the MEMS device in the range of 50 K to 400 K. The thermopower of BT NW was measured to be 56.8 μV/K while the electrical conductivity showed the value of 1.87×10^5 S/m at 300 K. The electrical conductivity of the NW increased with temperature decreasing, indicating a typical metallic behaviour.

In the thermal simulation result, it is shown that the actual temperature difference between the sensor contacts on the NW can be estimated using the simulation results. This methodology using a solid membrane pattern may provide an easy and high-throughput way to evaluate thermoelectric properties of various nanoscale objects such as thin NWs, as long as the thermal conductance of the target object is much smaller compared to that of the underlying membrane.

Acknowledgements

This work was supported by Future-based Technology Development Program (Nano Fields) through the National Research Foundation of Korea (NRF) funded by the Ministry of Education, Science and Technology (Grant No. 20110030200)".

6. REFERENCES

[1] L. D. Hicks and M. S. Dresselhaus, "Thermoelectric figure of merit of a one-dimensional conductor," *Physical Review B,* vol. 47, pp. 16631-16634, 1993.

[2] R. Sultan, A. D. Avery, G. Stiehl, and B. L. Zink, "Thermal conductivity of micromachined low-stress silicon-nitride beams from 77 to 325 K," *Journal of Applied Physics,* vol. 105, 2009.

[3] F. Nakamura, N. Taketoshi, T. Yagi, and T. Baba, "Observation of thermal transfer across a Pt thin film at a low temperature using a femtosecond light pulse thermoreflectance method," *Measurement Science and Technology,* vol. 22, 2011.